Controlling the Reaction Pathway to Tune Packaging Epoxy Properties

Polette Centellas
National Intitute of Standards and Technology
Gaithersburg, MD, USA
polette.centellas@nist.gov
ORCID: 0000-0003-3248-3409

Ran Tao
National Intitute of Standards and Technology
Gaithersburg, MD, USA
ran.tao@nist.gov
ORCID: 0000-0002-5208-7895

Andrew Korovich
National Intitute of Standards and Technology
Gaithersburg, MD, USA
andrew.korovich@nist.gov
ORCID: 0000-0003-3736-1523

Alexander K. Landauer
National Intitute of Standards and Technology
Gaithersburg, MD, USA
alexander.landauer@nist.gov
ORCID: 0000-0003-2863-039X

Amanda Forster
National Intitute of Standards and Technology
Gaithersburg, MD, USA
amanda.forster@nist.gov
ORCID: 0000-0001-7397-4429

Siena Iavarone-Garza
University of Maryland
College Park, MD, USA
siena.iavarone@gmail.com

Dante Ribeiro
Pennsylvania State University
University Park, PA, USA
danterib01@gmail.com

Huong Giang Nguyen
National Intitute of Standards and Technology
Gaithersburg, MD, USA
huong.nguyen@nist.gov
ORCID: 0000-0002-1052-7565

Jan Obrzut
National Intitute of Standards and Technology
Gaithersburg, MD, USA
jan.obrzut@nist.gov
ORCID: 0000-0001-6667-9712

Stian Romberg
University of Tennessee
Knoxville, TN, USA
sromberg@utk.edu
ORCID: 0000-0003-1026-2023

Christopher Soles
National Intitute of Standards and Technology
Gaithersburg, MD, USA
christopher.soles@nist.gov
ORCID: 0000-0002-1963-6039

2026 IEEE 76th Electronic Components and Technology Conference (ECTC) | USGov | DOI: 10.1109/ECTC51846.2026.00275

***Abstract*— Semiconductor packaging demands materials with simultaneously tuned properties. We demonstrate that the thermoset processing pathway influences functional properties, including moisture, dielectric, and thermomechanical responses. Using a model epoxy system, our findings establish pathway control as a lever to engineer thermoset performance for reliable semiconductor packaging.**

Keywords—epoxy thermoset, thermal curing, moisture uptake, dielectric response, coefficient of thermal expansion

I. Introduction

Thermoset polymers, such as epoxies, are indispensable in semiconductor packaging, serving as underfills, molding compounds, dielectric layers, and adhesives. As packages become more complex (ex. finer pitches, higher I/O counts, thinner components), these polymers are increasingly required to execute multiple functions concurrently. Beyond basic encapsulation and adhesion, they must provide environmental protection from moisture and ionic contamination, minimize electrical signal noise, and redistribute thermomechanical stresses generated by the coefficient-of-thermal-expansion mismatch across dissimilar materials in the package stack-up [1, 2, 3]. Key material attributes, including moisture sorption, dielectric properties, and thermal expansion, must be deliberately tuned to meet both process and lifetime requirements.

A central challenge is that these properties are not controlled solely by formulation; they also depend strongly on how the network is formed during curing. Thermoset epoxies are typically processed from low-viscosity monomers into crosslinked solids via thermally activated reactions. However, the thermal history can steer the reaction through different pathways, producing networks that are chemically similar yet structurally or topologically distinct. For example, curing above versus below the evolving glass transition temperature (T_g) can shift the system from a reaction-controlled regime to a diffusion-limited regime as vitrification occurs, altering the effective degree of conversion, crosslink density distribution, and degree of network heterogeneity [4, 5]. These structural differences influence free volume, segmental mobility, and the population of polar groups, features that directly affect the kinetics and thermodynamics of moisture uptake, dielectric behavior, and thermomechanical performance under service-relevant hygrothermal conditions. It is important to realize that controlling the reaction pathway provides a processing-based lever to tune epoxy performance without necessarily changing chemistry, enabling optimization strategies that are compatible with manufacturing constraints.

In this work, we demonstrate and quantify how reaction pathway control can be used to tailor packaging-relevant properties. Using a model epoxy thermoset, we systematically investigate three distinct reaction pathways designed to span curing scenarios relevant to packaging process windows (including conditions that promote or avoid vitrification during cure). We then connect the pathway-dependent network formation to the (i) moisture sorption/desorption behavior, (ii) dielectric constant and loss, and (iii) coefficient of thermal expansion, establishing a structure–processing–property framework that helps explain why nominally similar cures can yield meaningfully different reliability-critical responses. This approach provides practical guidance for selecting cure schedules that balance moisture resistance, dielectric properties, and mechanical integrity for advanced semiconductor packaging applications.

Official contribution of the National Institute of Standards and Technology; not subject to copyright in the United States.
National Institute of Standards and Technology Award # 70NANB24H283.

DOI 10.1109/ECTC51846.2026.00275

II. Experimental

A. Model Thermoset

We study a model thermoset system of bisphenol F diglycidyl ether (DGEBF) epoxy resin and diethyl toluene diamine (DETDA) curing agent. We select this chemistry for its industrial relevance as DGEBF epoxy is a foundational component of commercial underfill formulations [1, 2]. The resin components are individually degassed in a planetary mixer at a pressure of 100 mbar running at 2500 rpm for 5 min. The components are then combined at a stoichiometric ratio (2 equivalents DGEBF: 1 equivalent DETDA) and returned to the mixer for a second degassing and mixing step under identical conditions. The resin is used for testing within a few days of mixing. When not in use, it is stored in a freezer maintained at ca. 3 °C to minimize background curing.

B. Reaction Pathways

The model thermoset is cured using three different reaction pathways, i.e., cure schedules. Schedule A involves curing the material for 8 h at 120 °C. By maintaining the cure temperature below the glass transition temperature of the fully cured thermoset (T_g ~ 140 °C [6, 7]), we expect the material to slowly transition from its liquid state to a rubbery state to a glassy state (i.e., vitrify), resulting in a highly crosslinked network. Schedule B involves isothermal curing for 2 h at 150 °C. Curing at a temperature above the ultimate T_g will more quickly transition the material from its liquid state to a rubbery state, without vitrifying [4]. Schedule C involves curing the material for 1 h at 80 °C followed by 2.5 h at 150 °C. Multistep curing profiles that combine low- and high-temperature steps are commonly employed in composites manufacturing to minimize residual stresses [5]. All samples are cured in a convection oven with heating ramp rates of 5 °C min^{-1} and allowed to slowly cool to room temperature before being removed.

III. Material Characterization

A. Conversion Prediction

We develop a cure kinetics model to predict the evolution of the degree of conversion during thermal curing. First, we perform differential scanning calorimetry (DSC) dynamic heating scans on the uncured material from 40 °C to 315 °C at constant heating rates of (1, 3, 5, 10, 20) °C min^{-1}. The standard uncertainties for temperature and heat flow are approximately ± 1 % and ± 3 %, respectively. Then, we simultaneously fit the measured heat flow curves with a two-step reaction model using a commercial kinetic analysis software [8, 9, 10]. The validity of the two-step model is supported by literature, which describes the crosslinking of DGEBF with DETDA to first involve reaction with a primary amine to form a secondary amine, followed by a second reaction with the newly formed secondary amine [11]. The cure kinetics model is then used to predict the degree of conversion profile for each of the three reaction pathways.

B. Moisture Transport Properties

The moisture transport properties of the cured samples are measured using an isothermal vapor sorption analyzer. Free-standing films with an initial mass of ca. 13 mg and a thickness of ca. 120 μm are prepared for the experiments by sandwiching a small amount of resin between two glass plates lined with fluoroethylene-propylene (FEP) adhesive to prevent the epoxy from bonding to the substrates. Glass coverslips are placed around the deposited resin (in between the glass plates) to control the cured film thickness.

The cured films are conditioned for 240 min at 110 °C under pure nitrogen flow, i.e., 0 % relative humidity (RH). The sample environment is then set to run at (40, 60, 80, and 0) % RH in a stepwise manner at an isothermal temperature of 30 °C. The duration of each stage is 1200 min. Dry nitrogen is continuously mixed with a humid nitrogen flow to achieve the desired % RH. The instrument has a ± 0.1 μg mass resolution and ± 1 % RH control standard uncertainty. The mass change (M) is calculated relative to the dry mass measured at the end of the conditioning stage (m_{dry}) such that $M(t) = [m(t) - m_{dry}]/m_{dry}$.

The four sorption/desorption stages are simultaneously fit with Fick's one-dimensional diffusion model to extract the overall moisture diffusivity (D) and the saturated moisture content (M^{sat}) at each % RH stage [12],

$$M(t) = M_0 + (M^{sat} - M_0)\left[1 - \sum_{n=0}^{200} \frac{8}{{B_n}^2} \exp\left[-{B_n}^2 \frac{D(t - t_0)}{h^2}\right]\right] \quad (1)$$

where $B_n = (2n + 1)\pi$ and h is the film thickness. M_0 and t_0 are the mass change and time, respectively, corresponding to the start of the % RH stage. For example, the M_0 for the 60 % RH stage is equal to the M^{sat} for the 40 % RH stage.

C. Dielectric Response

Free-standing films for dielectric measurements are prepared using the same procedure described in the previous section for vapor sorption experiments. After curing, the film (ca. 300 μm thick) is carefully trimmed with a scalpel into a rectangle (3 – 6) mm-wide by (12 – 20) mm-long.

The dielectric constant and loss are measured using a non-contact microwave resonant cavity method described in IEC TS 62607-6-4:2024 [13, 14]. The epoxy film is inserted into an air-filled standard R100 rectangular waveguide (a = 10.16 mm, b = 22.86 mm, lz = 127.0 mm) connected to a network analyzer by two cross-polarized couplers, at the TE_{103} resonant frequency mode of 7.4543 GHz. Our previous work has shown that for a small sample inside a resonant cavity operating in a TE_{10n} mode,

$$\frac{f_0 - f_s}{f_0} = 2(\epsilon_r' - 1)\frac{V_s}{V_0} - b' \quad (2)$$

$$\frac{1}{Q_s} - \frac{1}{Q_0} = 4\epsilon_r''\frac{V_s}{V_0} - 2b'' \quad (3)$$

where the subscripts '0' and 's' refer to the empty and sample-filled cavity, respectively. f is the resonant frequency, V is the cavity volume ($V_0 >>> V_s$), and Q is the quality factor. ϵ_r' and ϵ_r'' are the real and imaginary components of the complex relative permittivity of the cavity space, and b' and b'' are related to the complex integral describing the non-uniform field in the specimen. The insertion of the specimen with permittivity $\epsilon_s^* = \epsilon_s' + j\epsilon_s''$ into the cavity results in a shift of the resonant

frequency from f_0 to f_s that is proportional to the dielectric constant of the specimen alone (ϵ_s'). It also results in a decrease of the quality factor from Q_0 to Q_s that is proportional to the dielectric loss factor of the specimen (ϵ_s''). The sample is partially inserted in 0.5 mm steps, controlled by a motorized stage, and the scattering parameter S_{21} is recorded at each step. From the recorded S_{21}, the cavity resonant frequency (f_s) is determined, and the quality factor is calculated from the conventional half-power bandwidth, $Q_s = f_s / \Delta f_s$. The components of the complex relative permittivity can then be calculated from plots of the frequency and quality factor versus insertion depth, using **Eq. 2** and **Eq. 3**.

D. Thermomechanical Response

The coefficient of thermal expansion (α) is measured using thermomechanical analysis (TMA), digital image correlation (DIC), and thin-film curvature techniques.

Untested, free-standing films prepared for vapor sorption experiments are used for TMA measurements. The sample is first heated from 25 °C to 110 °C and held for 20 min to remove moisture (drying step). It is then cooled to 25 °C to begin the TMA measurement and heated to 200 °C at 5 °C min^{-1} (first heating). The probe force is set to 0.02 N for the duration of the test, and the purge gas is N_2 at a flow rate of 50 mL min^{-1}. The coefficient of thermal expansion is calculated using the dimensional change measured between 35 °C and 100 °C from the first heating scan. The dimensional change is normalized by the value measured at 25 °C at the start of the heating scan.

For DIC measurements, a drop (about 40 mg) of epoxy is applied to a thin (ca. 0.03 mm) sheet of opaque high-temperature polyethylene terephthalate film and cured according to the three different cure schedules. After curing, the specimens are hemispherical disks about 7 mm in diameter and 1 mm in height at the center. The α of the relatively thin and compliant backer is estimated to have a negligible influence on the epoxy measurement compared to other uncertainty sources. The cured specimens are then sparsely speckled with black acrylic ink applied via airbrush, which generates uniformly distributed speckles roughly (4 to 7) pixels (px) in size. The speckled specimen and backer sheet are placed on a uniformly white substrate. To measure thermally induced strain, a stereo-DIC setup consisting of a pair of high-resolution machine vision cameras (ace2 a2A5328-15umPRO Monochrome, Basler AG) with 50 mm lenses (Fujinon CF50ZA1S, Fujifilm Corp.; set to f/4) and linear polarizing filters is paired with a modified convection/conduction reflow oven (GF-C2 from DDM NovaStar Inc) instrumented with an array of ungrounded K-type thermocouples (TMP41xx, Phidgets Inc; resolution ±0.08 °C). A commercial DIC software (MatchID Inc.) is used with zero-normalized sum-of-square differences matching, subset size 31 px, step size 5 px, strain window 25 px (virtual strain gauge size 151 px), using cumulative reference updating, bi-cubic spline interpolation, Green-Lagrange Q9 strain formulation. Effects such as heat mirage and window reflections are minimized largely following the recommendations of the DIC Good Practices Guide [15]. Total strain uncertainty (zero displacement noise floor plus one standard deviation of variation over the nominally uniform measurement) is estimated to be ± 0.13 % strain. Specimens are heated from nominal room temperature (25 °C), held at 40 °C for 5 min, then heated at 3 °C min^{-1} to 75 °C, held for 5 min, allowed to cool at the natural rate of the oven to 40 °C, held for 5 min, and cycled this way twice more. Images and thermocouple data are collected at 0.2 Hz. The surface strain due to thermal expansion is computed as the mean magnitude of the Green-Lagrange strain tensor in the measurement region of interest on the surface of the specimen. The slope of the resultant strain-temperature curve is fitted in a least-squares sense using a first-order polynomial with least absolute residuals metric and 99 % confidence interval. Since DIC measures surface strain from the relative displacements of the speckles, the mean strain value is associated with the linear, rather than volumetric, α. For more details, see [16].

To prepare samples for curvature measurements, we spin-coat a thin film of the uncured material (ca. 12 μm thick) onto 100-mm diameter silicon wafers (ca. 300 um thick). Each coated wafer is cured in accordance with one of the cure schedules and then diced into (4 to 5) mm-wide × (80 to 90) mm-long cantilevers. The film-coated cantilever is clamped at one end and suspended under ambient conditions. The sample temperature (T) is recorded using a thermocouple that is in contact with the edge of the substrate, and the sample curvature (κ) is measured using a commercial multi-beam optical stress sensor. The curvature resolution is calculated to be 1.6×10^{-4} m^{-1}, or 6.10 km radius of curvature. We program a radiant heater to condition the sample for 5 min at 110 °C, before cycling between 40 °C and 70 °C for 10 cycles at ramp rates of 10 °C min^{-1}, then finally cooling to 30 °C. The film stress (σ) is calculated from the sample curvature using Stoney's formula [17], $\sigma = (\kappa h_s^2 M_s)/(6 h_f)$, where h_s and h_f are the substrate and film thickness, respectively, and $M_s = 181$ GPa [18] is the biaxial elastic modulus of the silicon substrate. The residual stress is defined as the average value over the last 5 min of the experiment during which the sample is maintained at ca. 30 °C.

The film stress is plotted versus sample temperature for the thermal cycling segment to extract the coefficient of thermal expansion of the epoxy film (α_f) according to [9],

$$\alpha_f = \alpha_s - \frac{\Delta\sigma/\Delta T}{M_f} \tag{4}$$

where $\alpha_s = 2.6 \times 10^{-6}$ K^{-1} [18] is the coefficient of thermal expansion of the silicon substrate, $M_f = 3.1$ GPa [19] is the assumed biaxial elastic modulus of the film, and $\Delta\sigma/\Delta T$ is the slope of the linear fit to the data.

IV. Results and Discussion

A. Degree of Conversion Profiles

Fig. 1 shows the predicted degree of conversion profile for each cure schedule. The material is initially uncured (0 % conversion) before the reaction initiates at around 70 °C, or 9 min into the heating ramp, which is consistent across all profiles. For cure schedules A (**Fig. 1a**) and B (**Fig. 1b**), the rate of conversion accelerates after the reaction initiates and then decelerates after reaching either 120 °C or 150 °C, respectively. Cure schedule C (**Fig. 1b**) experiences a slower rate of conversion during the ramp and hold at 80 °C, which then accelerates upon heating to 150 °C, before decelerating

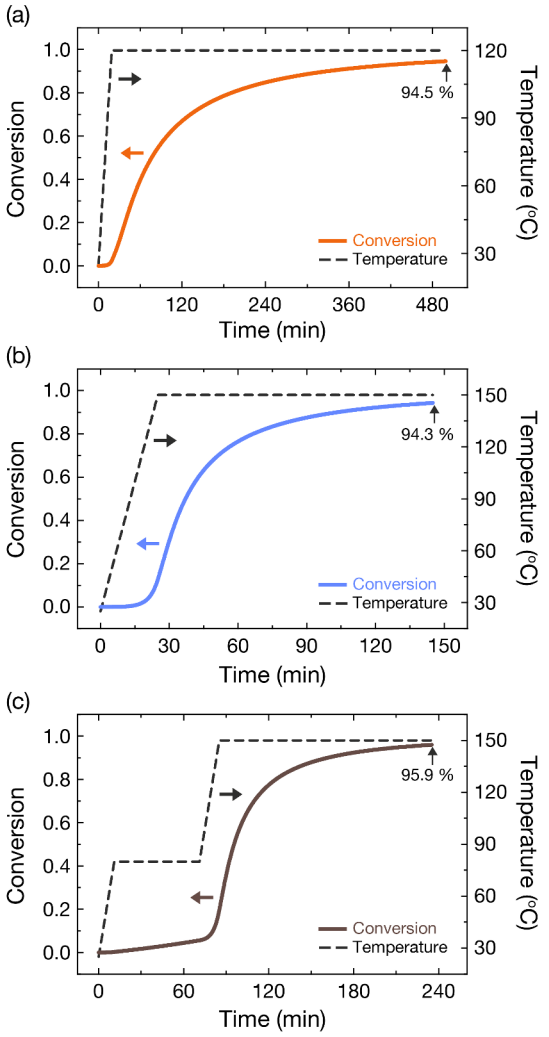

Fig. 1 Predicted degree of conversion profiles for the (a) low-temperature cure schedule A, (b) high-temperature cure schedule B, and (c) two-stage cure schedule C.

after this second isothermal hold. The degree of conversion at the end of schedule A is 94.5 %. Schedule B achieves a similar degree of conversion (94.3 %) despite a much shorter cure time (2 h versus 8 h) due to a faster conversion rate at a hotter isothermal hold (150 °C versus 120 °C). Schedule C, which combines low- and high-temperature isothermal holds, achieves a slightly higher conversion of 95.9 %. Therefore, we expect samples cured under schedule C to have a more extensive crosslinked network compared to samples cured under schedules A or B. However, the current kinetics model incorporates only chemically controlled kinetics and does not account for diffusion-controlled effects; therefore, the predicted conversion may overestimate the actual degree of cure after vitrification.

B. Moisture Diffusivity and Saturated Moisture Content

Vapor sorption/desorption measurements are shown in **Fig. 2a**. Fick's diffusion model (**Eq. 1**) produces a strong fit to the experimental data for all three profiles. The moisture

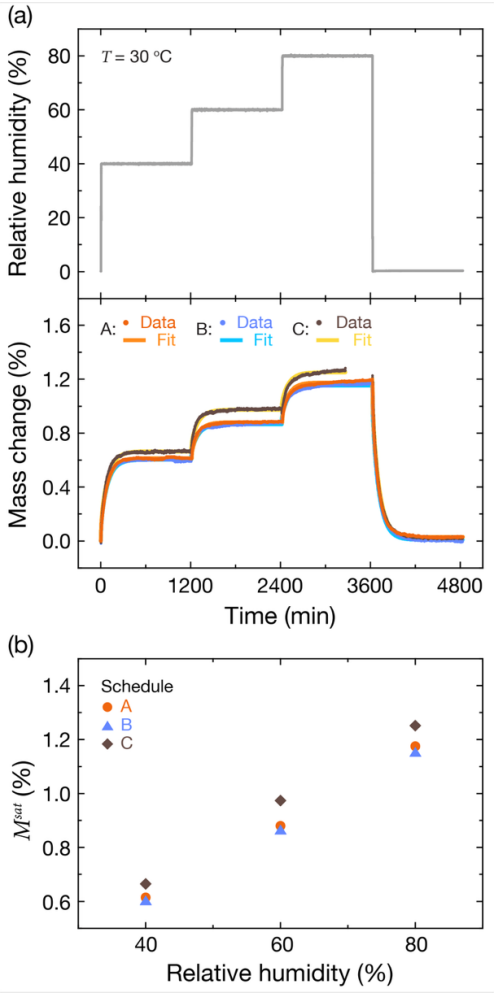

Fig. 2 Moisture sorption/desorption measurements for samples cured using schedule A (orange symbol), B (blue symbol), and C (brown symbol). (a) The mass change is measured during stepwise changes in the sample relative humidity (RH). The entire data set is fit with Fick's diffusion model to extract the overall moisture diffusivity and the saturated mass content (M^{sat}) at each % RH. (b) Extracted values of M^{sat} are plotted for the three sorption stages at (40, 60, and 80) % RH.

diffusivity values extracted from the fits are 2.93×10^{-7} mm^2 s^{-1} (standard error = 1.22×10^{-9} mm^2 s^{-1}) for schedule A, 2.56×10^{-7} mm^2 s^{-1} (standard error = 1.18×10^{-9} mm^2 s^{-1}) for schedule B, and 2.42×10^{-7} mm^2 s^{-1} (standard error = 1.40×10^{-9} mm^2 s^{-1}) for schedule C. The sample cured using schedule C uptakes more moisture upon saturation at each sorption stage (40 % RH, 60 % RH, 80 % RH) compared to samples cured using schedules A or B; this increase in M^{sat} is approximately 9 % (**Fig. 2b**). All samples lose nearly all their adsorbed moisture ($M^{sat} < 0.05$ %) by the end of the desorption stage (0 % RH). The extracted D and M^{sat} values are comparable to literature values for similar DGEBF-based epoxy systems [20, 21].

The primary driver for moisture uptake in epoxy systems is the network polarity, while a secondary driver is the nanovoid

structure [22, 23, 24]. The reaction of DGEBF with DETDA forms hydroxyl groups, secondary amines, and tertiary amines [11], which are polar sites in the thermoset network. These polar sites interact with and trap water molecules to slow down the kinetics of water diffusion but ultimately increase the amount of moisture uptake upon saturation. Therefore, increasing the degree of conversion increases the number of polar sites, which should reduce D but increase M^{sat}. Furthermore, nanovoids can facilitate the mobility of water molecules in the epoxy network to improve their accessibility to polar sites and thereby enable additional water uptake [22, 23]. Interestingly, molecular dynamic simulations predict an increase in the amount of size-matched nanovoids (i.e., larger than the kinetic diameter of a water molecule) as epoxy curing progresses [26]. In agreement with these theories, we find the smallest value for D and the largest values for M^{sat} (for the sorption stages) to correspond to the sample with the greatest predicted degree of conversion (schedule C). The sample cured using schedule A shows a slight, but statistically significant, increase in D and similar M^{sat} values compared to schedule B, which suggests a difference in mobility of polar functional groups in the network, despite a similar predicted degree of conversion. This hypothesis is further probed in the following discussion section on the measured dielectric properties.

C. Dielectric Constant and Dielectric Loss

The dielectric constant (ϵ_s') and loss (ϵ_s'') of the sample cured at low temperature (schedule A) are $\epsilon_s' = 3.110$ and $\epsilon_s'' = 0.1060$. The sample cured at high temperature (schedule B) exhibits lower values, with $\epsilon_s' = 2.505 \pm 0.002$ and $\epsilon_s'' = 0.0794 \pm 0.0001$. The higher dielectric properties measured for the sample cured under schedule A indicate a greater number of polarizable groups or increased mobility of the polarizable groups, e.g. hydroxyl and secondary amines, compared to the sample cured under schedule B. Although our cure kinetics modeling predicts a similar degree of conversion for both schedules, this prediction may overestimate the actual degree of cure after vitrification. Consequently, differences in the degree of crosslinking may exist between the samples. A lower degree of crosslinking in the schedule A sample would lead to more mobile polar groups, consistent with the higher values measured for the dielectric constant and loss. This also agrees with the trend observed in moisture diffusivity measurements, as a less crosslinked network would facilitate faster water uptake. As the predicted degree of conversion between the schedules is very similar, more chemically specific analyses via Raman spectroscopy and solid-state nuclear magnetic resonance are planned to elucidate the subtle differences in chemical structure.

D. Coefficient of Thermal Expansion

TMA (**Fig. 3a**), DIC (**Fig. 3b**), and thin-film curvature measurements (**Fig. 3c**) are used to extract the coefficient of thermal expansion of the cured samples. The values of α_f obtained from TMA and curvature measurements fall within the expected range for neat epoxies, $60 - 80 \times 10^{-6}$ K^{-1} [25, 26, 27], while DIC measurements of α_f are above this range (**Fig. 3d**). TMA measurements suggest that the α_f values for the three cure schedules fall within a range of ca. 3×10^{-6} K^{-1}. Conversely,

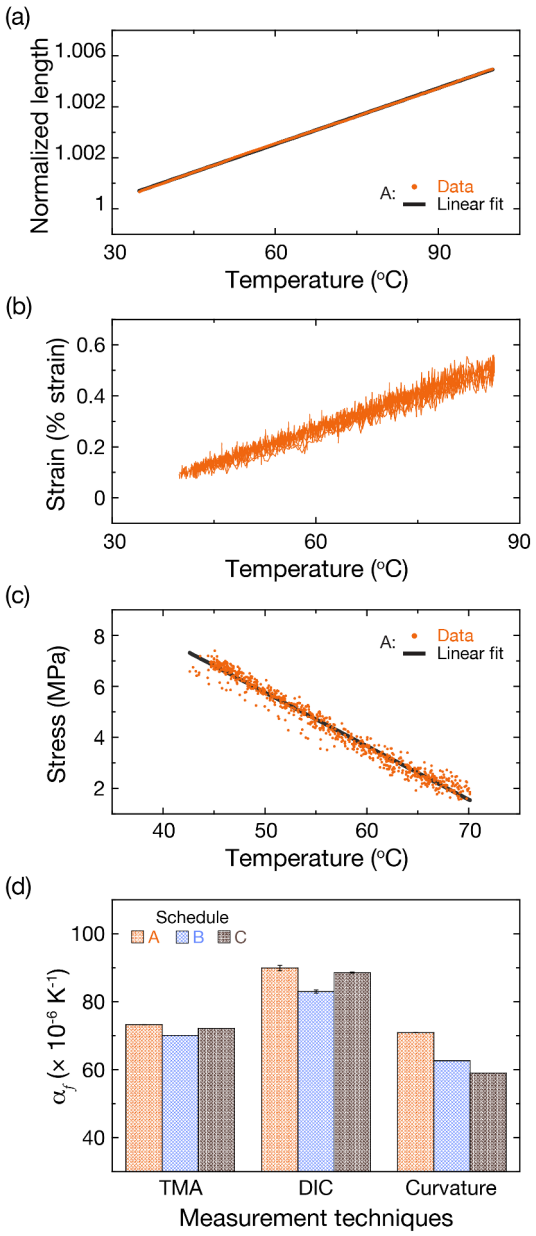

Fig. 3 Coefficient of thermal expansion (α_f) measurements for samples cured using schedule A obtained from (a) TMA, (b) DIC, and (c) thin-film curvature techniques. The solid lines for (a) and (c) are the linear fits to the data, where R = 0.999 and R = 0.987, respectively. (d) Comparison of α_f using the three techniques for the three cure schedules. The error from the linear fits for TMA and curvature measurements is too small to visualize on the plot. The error bars for DIC measurements represent the 99 % confidence intervals. One sample is measured for each test.

the curvature measurements suggest larger differences between samples. In particular, schedule C has the lowest value of α_f, which agrees with the theory that α_f is inversely proportional to the degree of conversion [30]. Further study is needed to identify

the best technique to accurately measure the α_f for this model system, but an initial discussion is presented below.

Each technique has its advantages and disadvantages. TMA is a well-established technique that directly measures small, temperature-induced dimensional changes. However, the measurement is sensitive to the contact force between the probe and the sample. Both DIC and thin-film curvature measurements are non-contact methods, which eliminates the possibility of mechanically deforming the sample during testing. The DIC approach requires application of a fine, uniform speckle pattern on the sample surface to resolve small changes in deformation [27], which may be challenging to achieve. Thin-film curvature measurements can resolve small deformations without modifying the sample, but the α_f analysis is highly sensitive to the assumed film modulus (**Eq. 4**). Therefore, this approach also requires an accurate measurement of the modulus, which is temperature-dependent. Geometric differences can also cause changes to cure (e.g., [29, 30]), which could explain the differences observed between trends in the curvature (thin film) measurements and TMA- and DIC-based (bulk) measurements of α_f. Utilizing different techniques to measure the coefficient of thermal expansion is a valuable approach to compensate for limitations in each individual technique.

E. Residual Stress

Thin-film curvature measurements are also used to compare the residual stress at room temperature ($T \sim 30$ °C) for each sample. Average values are (9.39 ± 0.09) MPa for schedule A, (8.52 ± 0.11) MPa for schedule B, and (12.02 ± 0.07) MPa for schedule C. As expected, the sample with the highest degree of conversion experiences the most cure shrinkage, which results in the greatest residual stress (schedule C). The difference in residual stress between schedules A and B is small, but statistically significant. One potential explanation for the lower stress measured in B compared to A is that it was cured at a higher isothermal temperature, where the increased thermal expansion of the resin could compete with the cure shrinkage to reduce the overall accumulated stress [5].

V. Conclusion

Results demonstrate that variations in the cure pathway can lead to potential differences in the moisture uptake behavior, dielectric response, and thermal expansion—properties that directly impact signal integrity, reliability, and service lifetime in advanced semiconductor packages. This work provides two key outcomes: (1) fundamental insight into how processing pathways alter thermoset network structures and package-relevant properties, and (2) a discussion of validated metrologies for reproducible, open-access characterization. By linking cure dynamics to performance-critical metrics, this study addresses urgent materials challenges and presents a potential strategy for utilizing thermoset processing protocols to enable next-generation semiconductor packaging.

Data Availability

Primary data associated with this paper are publicly available through the National Institute of Standards and Technology (NIST) Public Data Repository at [33].

Disclaimer

Certain equipment, instruments, software, or materials are identified in this paper to specify the experimental procedure adequately. Such identification is not intended to imply recommendation or endorsement of any product or service by NIST, nor is it intended to imply that the materials or equipment identified are necessarily the best available for the purpose.

Acknowledgment

We thank Dr. Jeff Gotro (InnoCentrix) for his guidance and insight regarding the model resin formulation. P.J.C. thanks Dr. Edwin Chan and Dr. Jeremiah Woodcock for their help with sample preparation for curvature measurements. This work was performed with funding from the CHIPS Metrology Program, part of CHIPS for America, NIST, U.S. Department of Commerce.

References

[1] Gang Li and Yangyang Sun, "Underfill Materials," in *Interconnect and Wafer Bonding Technology*, World Scientific, 2019.

[2] Z. Plachý, A. Pražanová, K. Dušek, and A. Géczy, "Underfill: A Review of Reliability Improvement Methods in Electronics Production," *Polymers*, vol. 17, no. 16, p. 2206, Aug. 2025, doi: 10.3390/polym17162206.

[3] R. Tao *et al.*, "Material Needs and Measurement Challenges for Advanced Semiconductor Packaging: Understanding the Soft Side of Science," *IEEE Trans. Compon., Packag. Manufact. Technol.*, vol. 15, no. 10, pp. 2071–2082, Oct. 2025, doi: 10.1109/TCPMT.2025.3603484.

[4] J. B. Enns and J. K. Gillham, "Time–temperature–transformation (TTT) cure diagram: Modeling the cure behavior of thermosets," *J of Applied Polymer Sci*, vol. 28, no. 8, pp. 2567–2591, Aug. 1983, doi: 10.1002/app.1983.070280810.

[5] P. Prasatya, G. B. McKenna, and S. L. Simon, "A Viscoelastic Model for Predicting Isotropic Residual Stresses in Thermosetting Materials: Effects of Processing Parameters," *j compos mater*, vol. 35, no. 10, pp. 826–848, May 2001, doi: 10.1177/002199801772662424.

[6] J. L. Tack and D. M. Ford, "Thermodynamic and mechanical properties of epoxy resin DGEBF crosslinked with DETDA by molecular dynamics," *Journal of Molecular Graphics and Modelling*, vol. 26, no. 8, pp. 1269–1275, Jun. 2008, doi: 10.1016/j.jmgm.2007.12.001.

[7] Z. Tsinas, A. Krishnamurthy, Q. An, R. Tao, A. L. Forster, and A. M. Forster, "Effects of Hyperbranched Polyethylenimine on the Properties of Commercial Epoxy Resins for Composite Applications," *ACS Polym. Au*, vol. 6, no. 1, pp. 278–292, Feb. 2026, doi: 10.1021/acspolymersau.5c00141.

[8] A. P. Kotula, R. Tao, J. Tu, Y. J. Lee, and G. A. Holmes, "Advanced Characterization of the Cure Kinetics of a Liquid Encapsulant," in *2025 IEEE 75th Electronic Components and Technology Conference (ECTC)*, Dallas, TX, USA: IEEE, May 2025, pp. 1784–1790. doi: 10.1109/ECTC51687.2025.00303.

[9] P. Centellas *et al.*, "Advanced Metrology Suite for Linking Residual Stress to Fundamental Properties of Thermoset Packaging Materials," in *2025 IEEE 75th Electronic Components and Technology Conference (ECTC)*, Dallas, TX, USA: IEEE, May 2025, pp. 432–439. doi: 10.1109/ECTC51687.2025.00078.

[10] C. Strasser, E. Moukhina, and J. Hartmann, "Time–temperature-transformation (TTT) cure diagram of an epoxy–amine system," *Macromol. Theory Simul.*, vol. 33, no. 6, 2024, doi: 10.1002/mats.202400039.

[11] S. U. Patil, S. P. Shah, M. Olaya, P. P. Deshpande, M. Maiaru, and G. M. Odegard, "Reactive Molecular Dynamics Simulation of Epoxy for the Full Cross-Linking Process," *ACS Appl. Polym. Mater.*, vol. 3, no. 11, pp. 5788–5797, Nov. 2021, doi: 10.1021/acsapm.1c01024.

[12] K. M. B. Jansen, M. F. Zhang, L. J. Ernst, D.-K. Vu, and L. Weiss, "Effect of temperature and humidity on moisture diffusion in an epoxy moulding

compound material," *Microelectronics Reliability*, vol. 107, p. 113596, Apr. 2020, doi: 10.1016/j.microrel.2020.113596.
[13] "IEC-TS-62607-6-4-2024."
[14] J. Obrzut, J. A. Clark, A. E. Baumann, and J. F. Douglas, "Dielectric Characterization of H_2 O and CO_2 Uptake by Polyethylenimine Films," *Langmuir*, vol. 40, no. 16, pp. 8562–8567, Apr. 2024, doi: 10.1021/acs.langmuir.4c00247.
[15] E. M. C. Jones and M. A. Iadicola, "A Good Practices Guide for Digital Image Correlation, Edition 2." 2025. doi: 10.32720/idics/gpg.ed2.
[16] A. Landauer, "A digital image correlation-based research platform for cure shrinkage and thermal expansion measurements on epoxy test materials," in *2026 IEEE 75th Electronic Components and Technology Conference (ECTC)*,
[17] L. B. Freund, J. A. Floro, and E. Chason, "Extensions of the Stoney formula for substrate curvature to configurations with thin substrates or large deformations," *Applied Physics Letters*, vol. 74, no. 14, pp. 1987–1989, Apr. 1999, doi: 10.1063/1.123722.
[18] J. J. Kim, G. R. Stafford, C. Beauchamp, and S. A. Kim, "Development of a Dental Implantable Temperature Sensor for Real-Time Diagnosis of Infectious Disease," *Sensors*, vol. 20, no. 14, p. 3953, Jul. 2020, doi: 10.3390/s20143953.
[19] S. U. Patil *et al.*, "Simple and convenient mapping of molecular dynamics mechanical property predictions of bisphenol-F epoxy for strain rate, temperature, and degree of cure," *Soft Matter*, vol. 19, no. 35, pp. 6731–6742, 2023, doi: 10.1039/D3SM00697B.
[20] C. Gillet, F. Tamssaouet, B. Hassoune-Rhabbour, T. Tchalla, and V. Nassiet, "Parameters Influencing Moisture Diffusion in Epoxy-Based Materials during Hygrothermal Ageing—A Review by Statistical Analysis," *Polymers*, vol. 14, no. 14, p. 2832, Jul. 2022, doi: 10.3390/polym14142832.
[21] A. Toscano, G. Pitarresi, M. Scafidi, M. Di Filippo, G. Spadaro, and S. Alessi, "Water diffusion and swelling stresses in highly crosslinked epoxy matrices," *Polymer Degradation and Stability*, vol. 133, pp. 255–263, Nov. 2016, doi: 10.1016/j.polymdegradstab.2016.09.004.
[22] C. L. Soles, F. T. Chang, B. A. Bolan, H. A. Hristov, D. W. Gidley, and A. F. Yee, "Contributions of the nanovoid structure to the moisture absorption properties of epoxy resins," *J. Polym. Sci. B Polym. Phys.*, vol. 36, no. 17, pp. 3035–3048, Dec. 1998, doi: 10.1002/(SICI)1099-0488(199812)36:17<3035::AID-POLB4>3.0.CO;2-Y.
[23] C. L. Soles, F. T. Chang, D. W. Gidley, and A. F. Yee, "Contributions of the nanovoid structure to the kinetics of moisture transport in epoxy resins," *J. Polym. Sci. B Polym. Phys.*, vol. 38, no. 5, pp. 776–791, Mar. 2000, doi: 10.1002/(SICI)1099-0488(20000301)38:5<776::AID-POLB15>3.0.CO;2-A.
[24] C. L. Soles and A. F. Yee, "A discussion of the molecular mechanisms of moisture transport in epoxy resins," *J. Polym. Sci. B Polym. Phys.*, vol. 38, no. 5, pp. 792–802, Mar. 2000, doi: 10.1002/(SICI)1099-0488(20000301)38:5<792::AID-POLB16>3.0.CO;2-H.
[25] M. D. Garrison, J. W. Tsang, and M. C. Davis, "Moisture Uptake and Thermomechanical Behavior of Epoxy–Amine Networks Derived from Ortho-Substituted Monomers," *ACS Appl. Polym. Mater.*, vol. 2, no. 7, pp. 2736–2748, Jul. 2020, doi: 10.1021/acsapm.0c00322.
[26] C. Li and A. Strachan, "Free volume evolution in the process of epoxy curing and its effect on mechanical properties," *Polymer*, vol. 97, pp. 456–464, Aug. 2016, doi: 10.1016/j.polymer.2016.05.059.
[27] A. G. Khina, D. P. Bulkatov, I. P. Storozhuk, and A. P. Sokolov, "Coefficient of Linear Thermal Expansion of Polymers and Polymer Composites: A Comprehensive Review," *Polymers*, vol. 17, no. 23, p. 3097, Nov. 2025, doi: 10.3390/polym17233097.
[28] M. Sadeghinia, K. M. B. Jansen, and L. J. Ernst, "Characterization and modeling the thermo-mechanical cure-dependent properties of epoxy molding compound," *International Journal of Adhesion and Adhesives*, vol. 32, pp. 82–88, Jan. 2012, doi: 10.1016/j.ijadhadh.2011.10.007.
[29] L. Khoun, T. Centea, and P. Hubert, "Characterization Methodology of Thermoset Resins for the Processing of Composite Materials — Case Study: CYCOM 890RTM Epoxy Resin," *Journal of Composite Materials*, vol. 44, no. 11, pp. 1397–1415, Jun. 2010, doi: 10.1177/0021998309353960.
[30] O. G. Kravchenko, C. Li, A. Strachan, S. G. Kravchenko, and R. B. Pipes, "Prediction of the chemical and thermal shrinkage in a thermoset polymer," *Composites Part A: Applied Science and Manufacturing*, vol. 66, pp. 35–43, Nov. 2014, doi: 10.1016/j.compositesa.2014.07.002.
[31] S. Yamamoto, R. Kuwahara, and K. Tanaka, "Interfacial Structure of Epoxy Resins on Amorphous Silica Surface under Dry and Wet Conditions," *J. Soc. Rheol., Jpn*, vol. 52, no. 2, pp. 91–98, Apr. 2024, doi: 10.1678/rheology.52.91.
[32] S. Yamamoto, N. T. Phan, K. Kihara, A. Shundo, and K. Tanaka, "Off-stoichiometry effect on the physical properties of epoxy resins," *Polym J*, vol. 57, no. 4, pp. 357–366, Apr. 2025, doi: 10.1038/s41428-024-00983-w.
[33] P. Centellas, R. Tao, A. Korovich, and A. Landauer, "Data for Controlling the Reaction Pathway to Tune Packaging Epoxy Properties." NIST Public Data Repository. doi: https://doi.org/10.18434/mds2-4101.